Supplementary Information

A new cation- and vacancy-ordered Brownmillerite in the Ba–In–Fe–O system revealing hidden order in its cubic counterpart

Monica Ceretti,*[a] Gabriel J. Cuello,[b] Denis Sheptyakov,[c] Anna Marsicano,[d] and Werner Paulus[a]

a. *ICGM, Univ Montpellier, CNRS, ENSCM,34000 Montpellier, France*
b. *Institut Laue-Langevin, 38042 Grenoble, France.*
c. *PSI, Center for Neutron and Muon Sciences, Villigen CH-5232, Switzerland*
d. *ISIS Neutron and Muon Facility, Rutherford Appleton Laboratory, Chilton, OX11 OQX, UK*

* Corresponding author: monica.ceretti@umontpellier.fr

Synthesis

Polycrystalline BFIO compounds were prepared by classical solid-state chemistry synthesis at high temperature. High purity $BaCO_3$ (99+%, ThermoScientific), In_2O_3 (99,995%, ALFA AESAR) and Fe_2O_3 (Puratronic 99,998%, ALFA AESAR) were thoroughly mixed and heated in air at 1200°C for 48 h, with intermediate grinding, to obtain the deficient cubic perovskite phase (BFIO-C in the following). The brownmillerite phase (BFIO-BM in the following) has been obtained by heating the cubic perovskite counterpart at 1000°C for four days in UHV (10^{-7} mbar) and then furnace cooling (about 5 °C/min) down to room temperature.

X-ray and neutron diffraction.

Phase purity were checked by laboratory X-ray powder diffraction on a Panalytical diffractometer in Bragg Brentano geometry using Cu_{Ka} radiation. Neutron powder diffraction (NPD) measurements were performed on the high-resolution diffractometer HPRT powder diffractometer[1] at SINQ spallation

neutron source of the Paul Scherrer Institute (λ = 1.494 Å). Diffraction data were analysed using the Rietveld refinement method implemented in the FullProf suite.[2]

Neutron PDF Diffraction

Neutron total scattering data for both compounds, BFIO-BM and BFIO-C, was collected on the disorder materials diffractometer D4c[3] at ILL (Grenoble, France) with an incident neutron wavelength λ = 0.4989 Å, covering a Q range between 0.35 and 23.5 $Å^{-1}$, at room temperature.[4]

The reduction and merging of the raw neutron data to obtain the pair distribution function G(r) was carried out using the software procedure ToScaNA developed at D4c.[5] The fitting of the *G(r)* was performed using the program PDFgui, a small-box modelling real-space 'Rietveld' refinement program.[6,7]

Magnetic measurements.

Magnetization measurements were performed with a superconducting quantum interference device (SQUID) magnetometer MPMS 7XL (Quantum Design magnetic property measurement system). Measurements were made by the dc method with a constant applied magnetic field of 1000 Oe from 2 to 300 K. The magnetic hysteresis loops were measured by recording the magnetization as a function of the applied magnetic field over a symmetric field range (±5 T) at 300K and 15K. Data were corrected using the Pd standard, taking advantage of its diamagnetic stability and negligible magnetic moment for accurate baseline calibration.

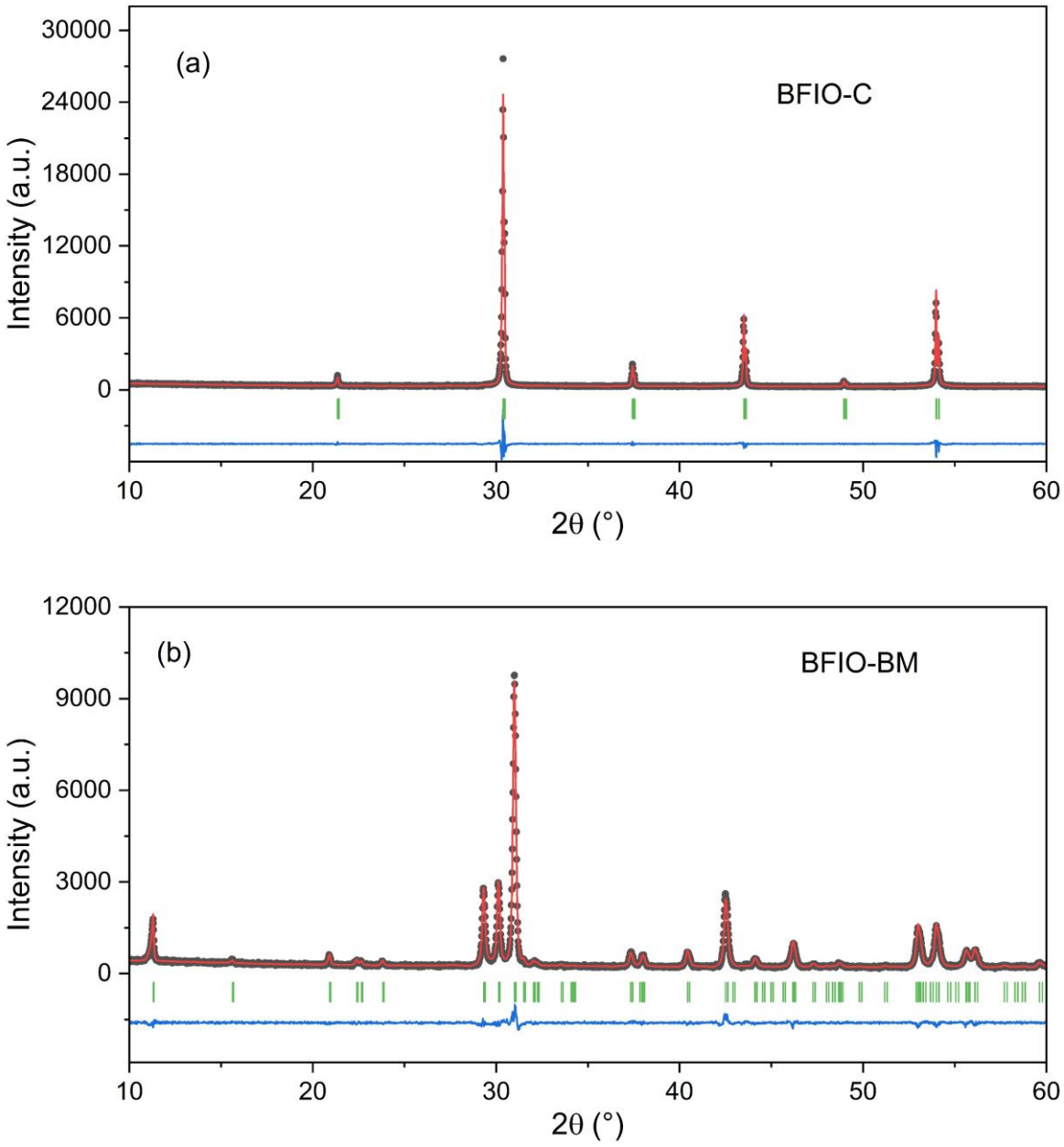

Figure S1 : Powder X-ray diffraction patterns and Rietveld refinements for BFIO-C and BFIO-BM (λ $Cu_{K\alpha 1}$)

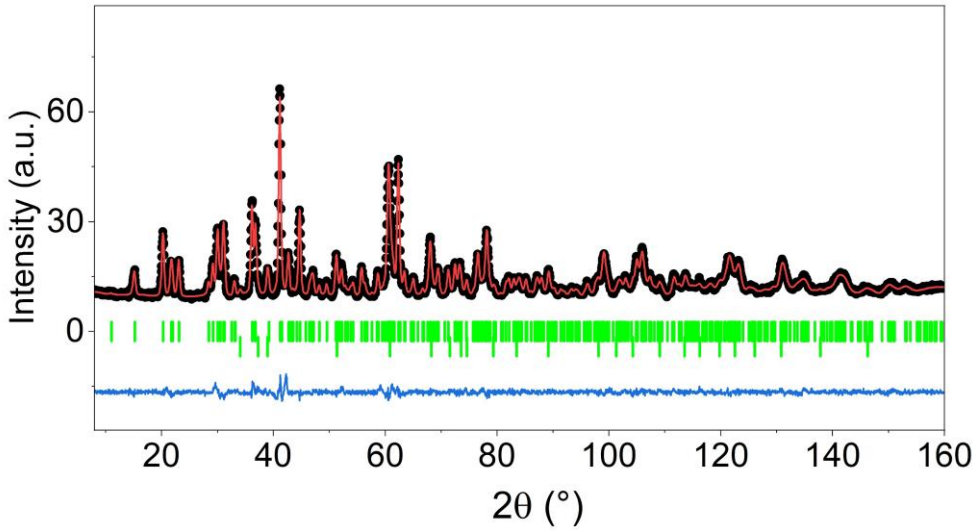

Figure S2: Rietveld refinements of NPD data at RT of *Imma* BFIO-BM. Black dots are the experimental data while the calculated patterns are represented by continuous red lines. The blue continuous line represents the difference between the experimental and calculated intensities. The short green vertical bars indicate the Bragg structural peaks of the BFIO-BM phase (the uppermost ones) and the sample holder (the lowermost ones).

Table S1: Structure data obtained from NPD Rietveld refinement of BFIO-BM at RT, in the *Imma* space group

Elements	x/a	y/b	z/c	U_{iso} (Å^2)	Occupancy	Site
Ba	½	0.8822(2)	0.0023(5)	0.0054(4)	1	8*h*
In	0	0	0	0.0091(4)	0.98(3)	4*a*
Fe	1.0061(7)	¼	0.0614(4)	0.0036(6)	0.51(3)	8*i*
O(1)	¼	0.0123(2)	¼	0.0049(5)	1	8*g*
O(2)	0	0.8561(2)	0.0697(4)	0.0127(5)	1	8*h*
O(3)	0.7334(7)	¾	0.7697(6)	0.0075(10)	1	8*i*

Imma	*a* (Å)	*b* (Å)	*c* (Å)	R_{Bragg} = 2.42%
Lattice parameters	5.9413(4)	15.7352(2)	6.1014(1)	R_{wp} = 3.85% R_p = 2.86% χ^2 = 1.94

Table S2 : Bond distances (in Å) and angles in Ba_2FeInO_5 from NPD at room temperature in the *I2mb* space group

Ba-O1	2.963(12)	In-O1(x2)	2.144(8)	Fe-O2(x2)	1.854(4)
Ba - O1	2.741(13)	In-O1(x2)	2.130(8)	Fe-O3	1.91(2)
Ba - O1	2.684(13)	In-O2(x2)	2.304(3)	Fe-O3	1.85(2)
Ba - O1	2.911(12)				
Ba - O2	2.930(2)	O1-In-O1	92.3(7)	O2-Fe-O2	128.8(3)
Ba - O2	2.645(5)	O1-In-O1	179.6(7) x2	O2-Fe-O3	108.2(9) x2
Ba - O3	2.893(16)	O1-In-O1	88.1(3) x2	O2-Fe-O3	102.1(9) x2
		O1-In-O2	84.9(4) x2	O3-Fe-O3	104.5(2)
		O1-In-O2	90.4(4) x2		
		O1-In-O1	91.6(7)		
		O1-In-O2	95.0(4) x2		
		O1-In-O2	89.7(4) x2		
		O2-In-O2	173.2(3)		

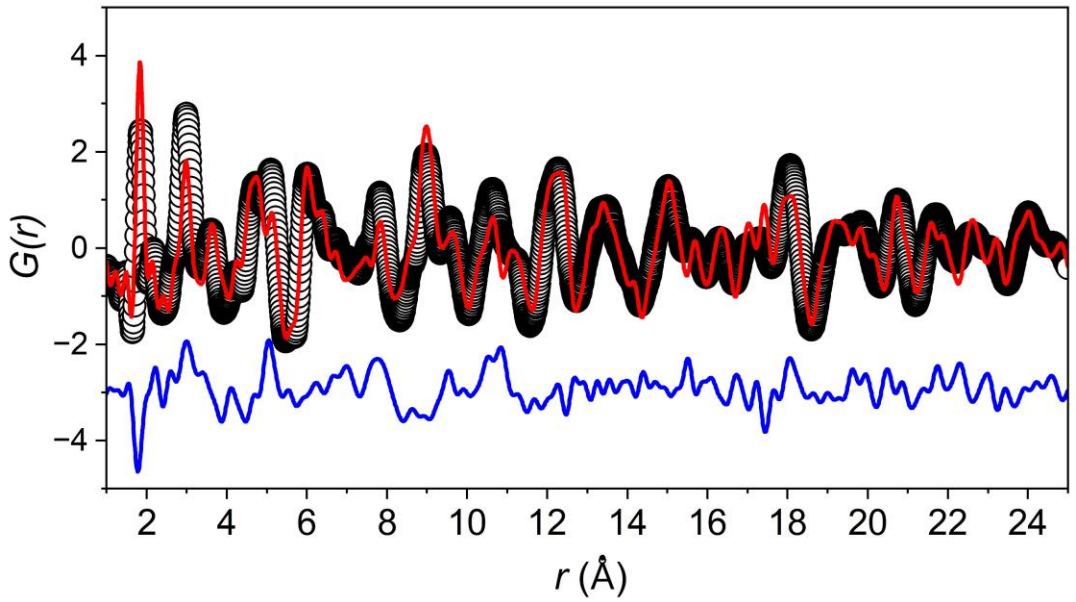

Figure S3 : PDFgui refinement (at room temperature) for orthorhombic BFIO-BM from *r* = 1 to 25 Å with the *Imma* model. This space group leads to a very poor refinement (*R*w = 43%), thus ruling out the *Imma* assignement.

Table S3: structural parameters of the orthorhombic BFIO-BM as obtained by PDF refinements at room temperature using the *I2mb* model. Lattice parameters: a = 5.9477(6) (Å), b = 15.7592 (10) (Å), c = 6.0953(9) (Å) (R_w = 18%)

Atom	*x*	*y*	*z*	U_{iso} (Å^2)
Ba	0.5058(10)	0.8825(14)	0.0045(7)	0.0072(4)
Fe	0.0025 (16)	0.25	0.0646(3)	0.0083(3)
In	0.00	0.00	0.00	0.0096(9)
O1	0.2492(10)	0.0112(1)	0.2642(9)	0.0075(7)
O2	0.0114(16)	0.8561(10)	0.06770(8)	0.0117(3)
O3	0.7655(20)	0.75	0.7499(13)	0.0101(2)

Table S4 Crystal structure parameters of BFIO-C from Rietveld neutron data refinements against the *Pm-3m* space group (Neutron diffraction data at room temperature, HRPT@PSI, λ = 1.494 Å). Lattice parameter: $a = b = c$= 4.15622(23) Å (R_p = 3.46%; R_{wp} = 4.41%; χ^2 = 1.51; R_f = 2.88)

Atom	*x*	*y*	*z*	*U* (Å^2)	*Occ.*
Ba	0.5	0.5	0.5	0.0244(6)	1
Fe/In	0.0	0.0	0.0	0.0589(7)	0.5/0.5
O	0.5	0.0	0.0	0.0538(8)	0.803(6)

The refined oxygen stoichiometry appears slightly lower than expected. This apparent reduction is likely an artifact of the Rietveld refinement process, where high thermal displacement parameters (temperature factors U) for oxygen atoms, combined with their correlation with occupancy, can lead to an underestimation of the actual oxygen content.

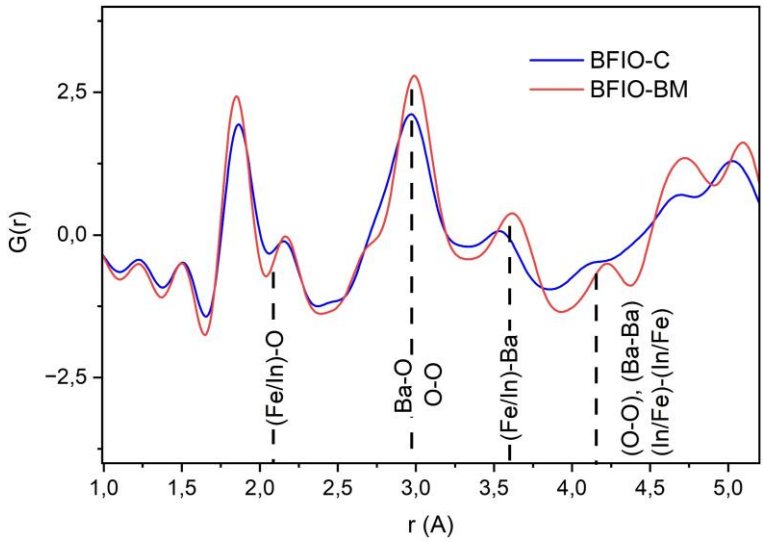

Figure S4: Low-*r* region of neutron PDF data at room temperature of the cubic (BFIO-C, blue line) and orthorhombic phase (BFIO-BM, red line). For comparison the single nearest interatomic distances calculated for the cubic perovskite are also reported (black dashed lines).

Table S5: Structural parameters of the cubic BFIO-C as obtained by PDF refinements at room temperature using the *I2mb* model, in the short range 1 Å < *r* < 5.5 Å. Lattice parameters: *a* = 5.7798(9) Å, *b* = 16.1574 (26) Å, *c* = 6.1612 (10) Å, (R_w = 8%).

Atom	*x*	*y*	*z*	U_{iso} (A^2)
Ba	0.5049(16)	0.8825(15)	0.0044(46)	0.0068 (23)
Fe	0.0101(16)	0.25	0.0644(29)	0.03799 (38)
In	0.00	0.00	0.00	0.0050 (20)
O1	0.248()	0.0117(15)	0.2596(61)	0.0058 (0.01)
O2	0.0120(15)	0.8562(10)	0.0678(10)	0.0150 (0.13)
O3	0.7656(17)	0.75	0.7492(13)	0.01351 (0.13)

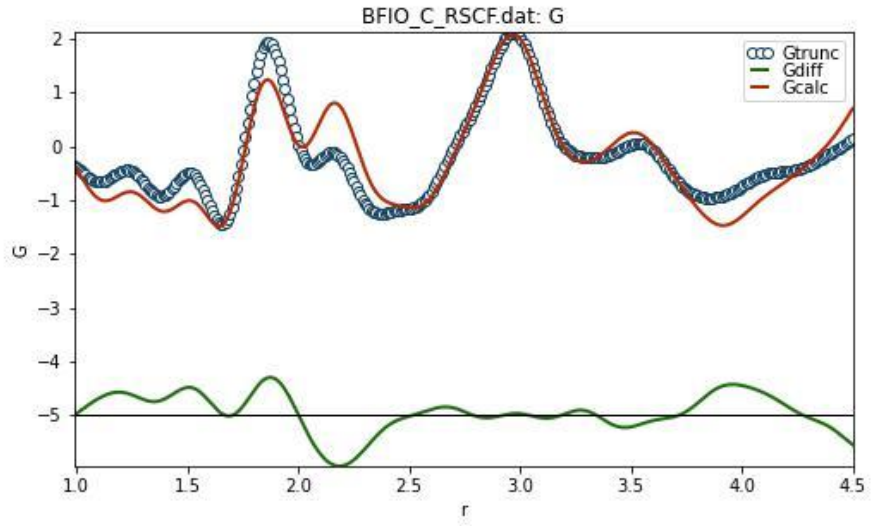

Figure S5 : Comparison of the experimental (blue circles) and calculated (red line) *G(r)* for cubic BFIO-C in the low-*r* region, using a structural model with 50% Fe and 50% In distributed over both octahedral and tetrahedral sites.

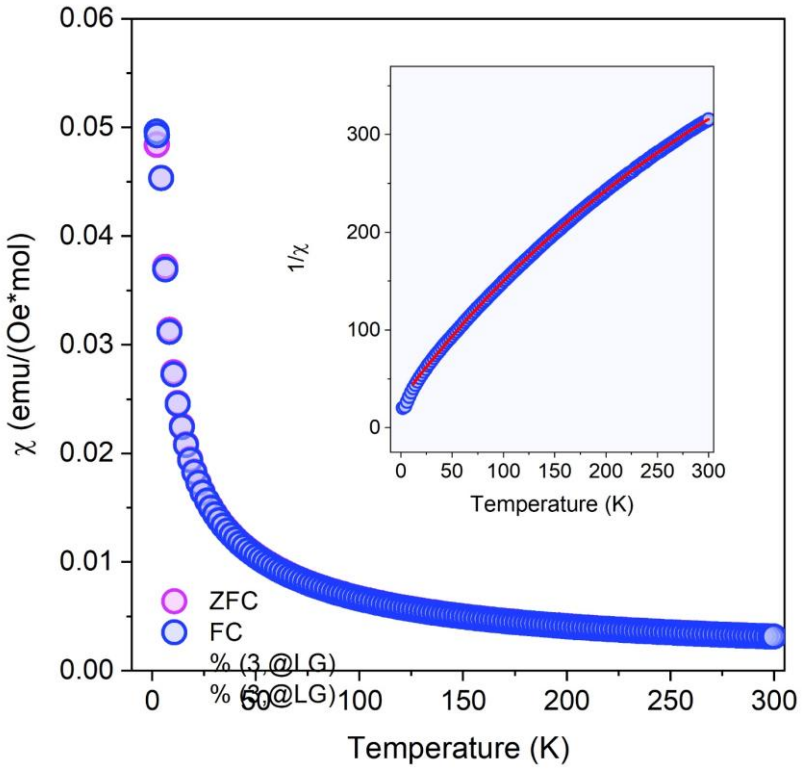

Figure S6 : Magnetic susceptibility for the cubic oxygen deficient perovskite BFIO-C measured under an applied field of 1000 Oe. In the inset, the inverse magnetic susceptibility, fitted with a modified Curie Weiss equation (in red), yielding a μ_{eff} = (5.59 ± 0.5) μ_B and χ_0 = (10.8 ± 0.1) x10^{-4} emu/(mole*Oe). Data are consistent with those reported in literature.[8]

x-ray : ordered Fe/In

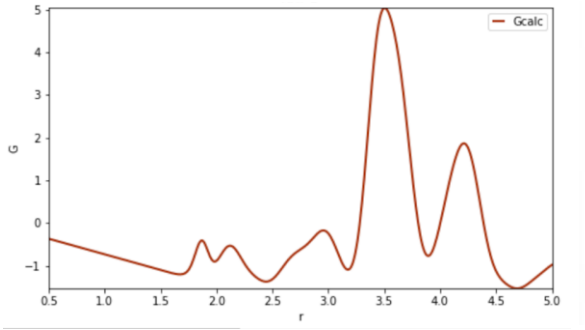

x-ray : disordered Fe/In

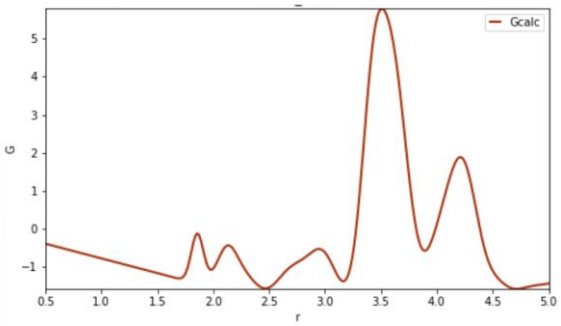

neutron : ordered Fe/In

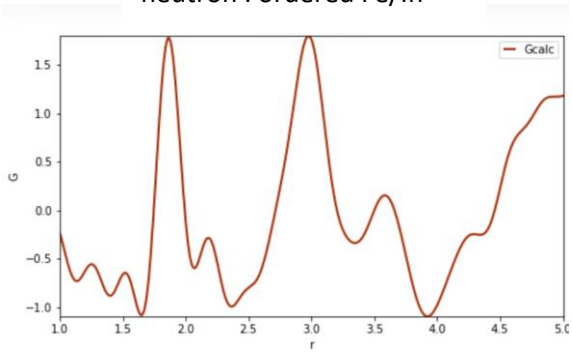

neutron : disordered Fe/In

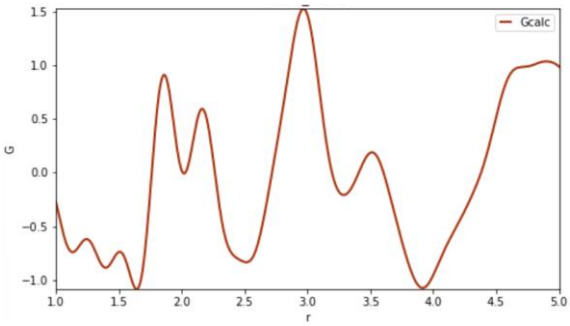

Figure S7: Simulated X-ray and neutron pdf patterns for cubic Ba_2InFeO_5, for an ordered and disordered Fe/In distribution. While there is hardly no difference in the X-ray case, neutron pdf shows a clear difference for both scenarios, underlining that X-ray diffraction does not allow to distinguish between an ordered or disordered B-cation distribution. Although the contrast between these two elements is comparable in X-ray and neutron scattering (with inverted signs), the decisive advantage of neutrons lies in their point-scatterer nature: the Q-independent scattering length ensures reliable scattering intensities up to high momentum transfers, translating directly into a substantially higher real-space structural resolution.

(a)

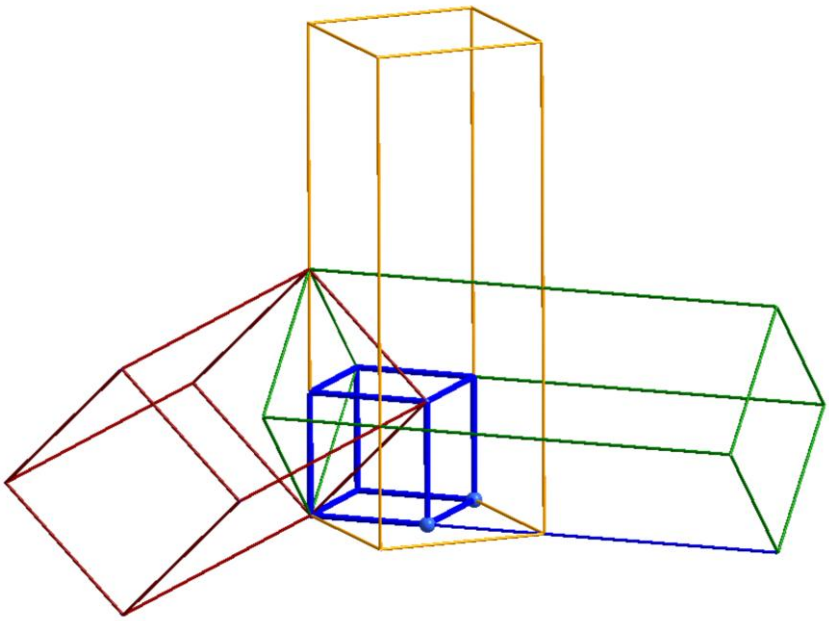

(b)

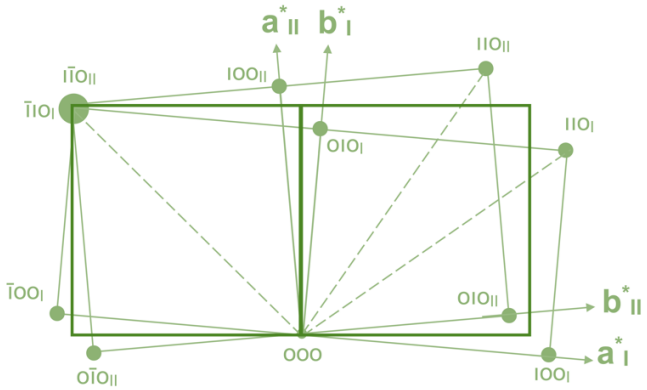

Figure S8: Domain formation in BFIO-C starting from the cubic perovskite (blue), showing 3 Brownmillerite unit cells with $a\sqrt{2}$ x $a\sqrt{2}$ x 4c, and for which each orientation variant can split into 4 orthorhombic twin domains (b), related to the slight difference in the *a/b* axes as outlined in [9].

References

1 P. Fischer, G. Frey, M. Koch, M. Könnecke, V. Pomjakushin, J. Schefer, R. Thut, N. Schlumpf, R. Bürge, U. Greuter, S. Bondt and E. Berruyer, *Physica B: Condensed Matter*, 2000, **276–278**, 146–147.

2 J. Rodríguez-Carvajal, *IUCr Newsletter*, 2001, **26**, 12-19. The complete FULLPROF suite can be obtained from: http://www.ill.eu/sites/fullprof/index.html.

3 H. E. Fischer, G. J. Cuello, P. Palleau, D. Feltin, A. C. Barnes, Y. S. Badyal and J. M. Simonson, *Applied Physics A: Materials Science & Processing*, 2002, **74**, s160–s162.

4 M. Ceretti, G. Cuello and W. Paulus, *Exploring Proton Conductivity Mechanisms In Oxygen Deficient Perovskites $SrSc_{0.5}Ga_{0.5}O_{2.5}$*, 2024, Institut Laue-Langevin (ILL), doi:10.5291/ILL-DATA.6-06-532.

5 G. J. Cuello, ToScaNA: Total Scattering Neutron Analysis 2025.
6 Th. Proffen and S. J. L. Billinge, *J Appl Crystallogr*, 1999, **32**, 572–575.
7 C. L. Farrow, P. Juhas, J. W. Liu, D. Bryndin, E. S. Božin, J. Bloch, T. Proffen and S. J. L. Billinge, *J. Phys.: Condens. Matter*, 2007, **19**, 335219.
8 A. D. Lozano-Gorrín, B. Wright, P. A. Dube, C. A. Marjerrison, F. Yuan, G. King, D. H. Ryan, C. Gonzalez-Silgo, L. M. D. Cranswick, A. P. Grosvenor and J. E. Greedan, *ACS Omega*, 2021, **6**, 6017–6029.
9 A. Maity, R. Dutta, B. Penkala, M. Ceretti, A. Letrouit-Lebranchu, D. Chernyshov, A. Perichon, A. Piovano, A. Bossak, M. Meven and W. Paulus, *J. Phys. D: Appl. Phys.*, 2015, **48**, 504004.